Korean J. Chem. Eng., 40(4), 943-951 (2023)
DOI: 10.1007/s11814-022-1346-2

pISSN: 0256-1115
eISSN: 1975-7220

Microstructural and thermal investigation of the bioinspired and synthetic fire-retardant materials deposited on cotton using LBL process

Zeeshan Ur Rehman*, Ye-Tang Pan, David George Churchill***, and Bon Hen Koo*,†**

*College of Mechatronic Engineering, Changwon National University, Changwon, Gyeongsangnam-do 51140, Korea
**National Engineering Technology Research Center of Flame-Retardant Materials, School of Materials Science & Engineering, Beijing Institute of Technology, Beijing, 100081, P. R. China
***Department of Chemistry, Molecular Logic Gate Laboratory, Korea Advanced Institute of Science and Technology (KAIST), Deajon 34141, Korea
(*Received 18 May 2022 • Revised 8 November 2022 • Accepted 13 November 2022*)

Abstract−A detailed comparison of the bio- and synthetic polymers based layer by layer (LBL) coatings on a singular cotton fabric substrate was carried out. The growth of the deposited layers and subsequent properties, that could govern the fire protection of the substrate, were studied using low voltage-scanning electron microscope (LV-SEM) and thermal analysis techniques. From the 2D and 3D microstructural evaluation, uniform layered structure, agglomerated/precipitated structures and inter-fibers connecting layered-structure were explored, more thoroughly for chitosan and alginate based (CHI-2, ALG-2) biopolymer coatings, whereas the microstructure of synthetic polymers-based coatings ammonium polyphosphate and Polyvinyl Alcohol (APP-2 and PVA-2) showed only uniform layers. From the micro-thermal evaluation (TGA and MCC), a two-step degradation was recorded for all samples with a higher char residue recorded for APP-2 (TGA, ~39.2%, at 600 °C, MCC ~33.0% at 800 °C) followed by CHI-2 (TGA, ~12.5% at 600 °C, MCC, ~8.92% at 800 °C) suggesting superiority of the APP-2 based deposition over that of CHI-2. In addition, the same pattern of dominance was found consistent with the peak heat release rate (PHRR) values and total heat release (THR) values for APP~ (85.1 W/g, 6.53 KJ/g), and CHI-2~ (227.74 W/g, 17.17 KJ/g), respectively. However, from the VFT analysis, both samples were found to have comparable properties, in terms of structural integrations, char residue, and flame resistance.

Keywords: Microstructure, Synthetic Polymers, Biopolymers, Ammonium Polyphosphate, Chitosan, LBL Method, UL-94, Fire Retardant, MCC, HRR

INTRODUCTION

Due to several incomparable aspects, such as the noble texture and comfort, as well as excellent hygroscopicity, biodegradability, "breathability" and antistatic properties, cotton fabrics have remained vital to human life throughout human history [1-4]. The current modern technological and scientific innovations have made the use of cotton to a more sizable level due to its widespread applications in a diverse spectrum of products, ranging from high tech industry to the typical home commodities. However, this widespread use is always threatened by the fire vulnerability of cotton due to its intrinsic molecular structure. Among the major drawbacks of cotton and things composed of cotton are its low limiting oxygen index values (LOI~ 17-20%), higher specific heat release rate and lower degradation temperature (360-425 °C) [5].

Compared to other materials with fire retardant properties controllable through other means [6,7], cotton is a natural material, the options utilized to attenuate its vulnerabilities continue to be limited, i.e., intrinsic weak flame-retardant properties need to be mitigated. Some of the techniques that can be used and have been investigated so far can be listed as surface grafting technique [8], ultraviolet curing of deposited polymers on cotton [9], flame retardant finishing treatment [10], sol-gel methods of thin-film deposition [11], plasma treatments [12], and the layer-by-layer (LBL) coating technique [13-17]. Among these, a layer-by-layer approach, to prepare fire retardant coating is a relatively new technique, that can produce nano-level thin films on cotton fabric as well as on other fire-vulnerable substrates. In recent decades the LBL approach has been extensively investigated by multiple research communities [18,19].

The LBL process involves deposition of a coating on a substrate of interest either by (i) spraying or (ii) dipping the substrate alternatively into a dilute aqueous solution/mixture of polymers or particles based on polycations and polyanions (<1 wt% solids). Such an alternative periodic dipping/spraying process allows for a thin layer assembly of electrolytes layers (also known as bilayers, BL) formed on the substrate as a result of electrostatic interactions. The electrostatic interactions could also be co-assisted by other forces such as hydrogen bonding [20], donor/acceptor interactions [21], and covalent bonding [22] to help form these multilayered assemblies. The strength and scope of each of these forces has a strong dependency on the process parameters and nature of the electrolytes, such as the type of cationic solution [22], molecular weight of the component of the electrolyte [23], ionic and bond strength

†To whom correspondence should be addressed.
E-mail: bhkoo@changwon.ac.kr

[24], and lastly, pH and temperature of the working electrolytes [25]. Due to such experimental variables, coating thickness, which ranges from 1-100 nm, structure and degree of uniformity can be controlled.

Using a layer-by-layer process, numerous synthetic and biopolymers coupled with nanostructures, clay materials, graphene oxides and complex polyelectrolytes were deposited on the cotton to enhance the flame suppressing properties of the cotton. In regard to synthetic polyelectrolytes, common combinations used by various authors are poly(sodium phosphate) (PSP), poly(allylamine) (PAAm), poly(diallydimethylammonium chloride), polyacrylic acid (PAA), poly(diallydimethylammonium chloride) and APP [26,27]. In addition, polymer-particle coupled systems are also utilized to help impart fire retardant properties to the substrate materials. For instance, Carosio et al., applied two systems, Chitosan-APP and SiO_2-APP, in order to compare the role of each system [28]. In addition, other significant materials such as poly(vinylphosphonic acid) (PVPA), BPEI [29], and oligoallylamines/phosphonated oligoallylamines were deposited on the cotton fibers and the obtained thermal stability and flammability was examined [30]. Nanostructures such as TiO_2 nanoparticle [31,32], hydrotalcite nanoparticles [33] amino-functionalized MWNTs (MWNT-NH2) coupled with APP [34]. anionic Al_2O_3/cationic Al_2O_3 [35] were also deposited through LBL process for fire protection applications. Likewise, LBL coatings based on "green" materials, acquired from available bio feedstock, either plants or animal in origin, were obtained using anionic alginate (AL) [36] phytic acid [37] chitosan, lignin [38], tannic acid [39] deoxyribonucleic acid [40], cellulose nanofibers [41], starch [42,43] hydrophobins, whey protein and casein on textiles and other polymeric materials [44], [45]. The research further extended to plant extracts, like bananas pseudo-stem sap and spinach juice, and it was explored that depositing such extracts through exhaust method or layer-by-layer method, the limiting oxygen index (LOI) values of cotton fabrics could be improved up to 30% [46].

The assessment for the implementation of both classes of these materials revealed severe flaws, which inhibit their widespread application. Assessments involved in-depth calculations of variables pertinent to commerce. Major issues of concerns include (i) toxicity, (ii) mechanical shift in the original properties, (iii) cost burden and (iv) insufficient efficiency for green materials. Therefore, consistent efforts are underway to investigate and explore these materials in order to find optimum solutions for the fire retardant applications. Due to the wide variety of the substrate materials and their quality, various results of authors could not establish and investigated particular features related to green and synthetic materials. Thus, there is need to carry out a detailed comparative analysis of the green and synthetic materials-based LBL coatings on a singular substrate and establish standards for the thermal and protective properties of these materials. In addition, polyvinyl alcohol was used for the first time as electrolyte source for LBL process and compared with other polyelectrolytes source. Therefore, this report offers a one-stop investigation details of the thermal, structural growth and flammability properties of both synthetic and biopolymer-based coatings deposited on cotton fabric using LBL technique.

EXPERIMENTAL PROTOCOL

The substrate cotton fabric (100%, 180 g/m^2) was obtained from a local company and then cut into rectangular pieces with dimensions as ~230 mm/120 mm (height/width). Montmorillonite clay was obtained from Sigma Aldrich, polyacrylic acid solution (Fujifilm), polyvinyl alcohol (Sigma Aldrich), chitosan, low molecular

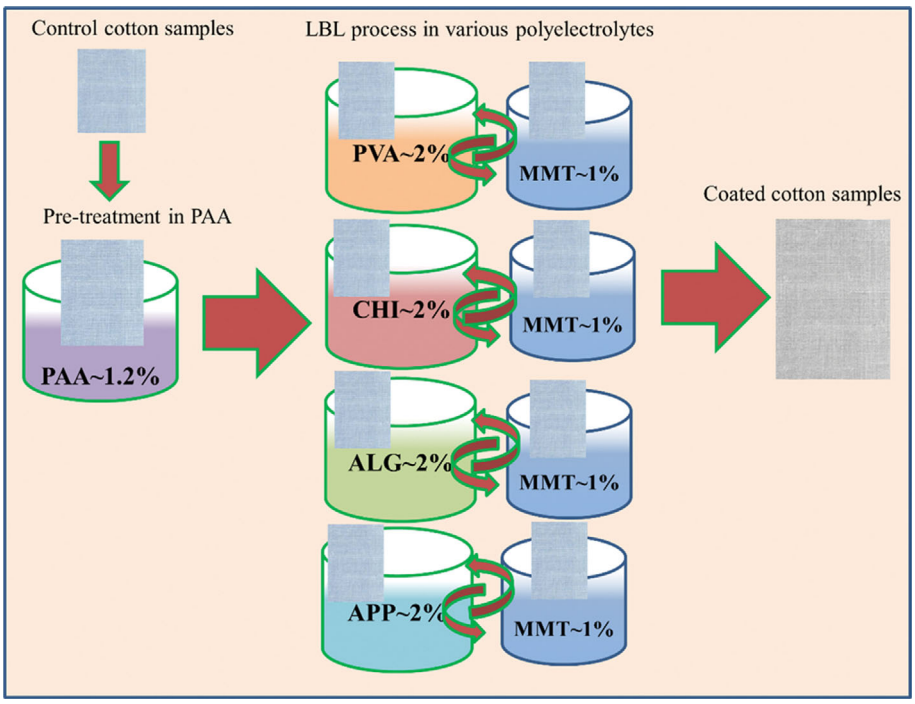

Fig. 1. Schematic diagram of depositing coating layers on cotton fabric using LBL process.

weight (Sigma Aldrich), alginic acid calcium salt (Sigma Aldrich) and ammonium poly phosphate (Sigma Aldrich) and DI water 18.6 Ω·cm. Coatings on the cotton fabric were deposited by alternate dipping process into cationic additives-based solutions and polyanionic MMT powder suspension. Before the coating process, the fabric was dipped in polyacrylic acid solution (1.2%, pH~1.8) for 20 minutes to allow for a surge in the (–ve) charge at the surface of the cotton fabric. After washing and drying, the fabric was then coated in each polycationic solution (polyvinyl alcohol, chitosan, alginic acid calcium salt and ammonium polyphosphate, each 2%) for 5 min. After each dipping step, rinsing in deionized water and hot air drying was conducted. The fabric was then dipped in the polyanionic clay solution (MMT, 1%) for 5 min. Finally, the coated samples were dried in an 80 °C oven for 2 h. The fabric was coated with a total number of seven bilayers. The initial bilayer required 5 min while the remaining Bilayers required 2 min. The obtained coated substrates were labelled as PVA-2, CHI-2, ALG-2, APP-2. The coatings process and intermediate steps are diagrammed in Fig. 1.

To analyze the microstructure, pre-coated and post coated samples were imaged. Renderings of the surfaces of the cotton samples were obtained using low voltage scanning electronic microscope (LV-SEM, Merlin compact). Surface images of the post-VFT (vertical flame test) char residues were also taken using LV-SEM. To help evaluate the elemental composition of the coated samples and post VFT char residue surfaces, EDAX analysis was carried out. Due to the lower conductivity of the samples, prior to each analysis the specimens were Pt-sputtered for about 2.5 min, under high vacuum to increase the conductivity. The micro-thermal properties of the specimens were analyzed using thermogravimeter instrument (Perkin Elmer Pyris-1 instrument, Massachusetts, USA) under the nitrogen atmosphere (20 ml min^{-1}), temperature range of 50-600 °C and heating rate ~20 °C min^{-1}. The amount of the sample used for each TGA count was 10-15 mg. Microscale combustibility (MCC) of the sample was examined using FTT Microscale combustion calorimeter (ASTM standard method D7309-2007 'Method B). The specimens, each weighing (10-15 mg) in platinum pans, were kept at 100 °C for 5 min, followed by a temperature increase up to 750 °C, under 20 : 80 O_2 : N_2 environment. The macro-thermal properties were explored using a vertical flame test, conducted for both pre- and post-coated specimens according to an ASTM D6413 protocol. For this purpose, a locally made chamber was used to burn the samples of approximate dimensions ~300 mm×120 mm. A butane torch flame, stabilized at 20 mm in length, was placed below the fabric sample for 10 sec to help the samples reach ignition point temperature. The flame spread properties, burning time, char properties were then measured from the data recorded by high-resolution optical camera (Samsung).

RESULTS AND DISCUSSION

1. Microstructural Analysis

Surface images of the LBL-coated and uncoated fabric mesh are presented in Figs. 2(a)-(e). The surface of the uncoated sample has a clean and highly smooth topology compared to the coated samples, which have rough, closely connected and layer-structured features, as can also be observed from the 3D surface plots provided in Fig. 3(a)-(h). The uniform layered structure of the fibers surfaces as indicated by "B" can be observed clearly in all the samples as Fig. 3(b)-(e). The layered structure is caused by the alternate deposition of the coating species. However, such layered structure cannot be observed in case of uncoated control samples such as in Fig. 3(a), suggesting successful deposition of the LBL coatings on the substrates. The coated fibers can also be seen as covered with the layers of agglomerated/precipitated structures, deposited inconsistently on the surface as encircled "A" in Fig. 2(c). Such agglomeration and precipitation are typical phenomena, occurring due to particle interaction of individual particles in the suspension [24]. The 3D plot of the agglomeration can be seen in Fig. 3(h), which suggests a uniform distribution of the constituent particles in the agglomeration packet. In addition, there can also be seen inter-fibers connecting layers caused by the deposition of the coating

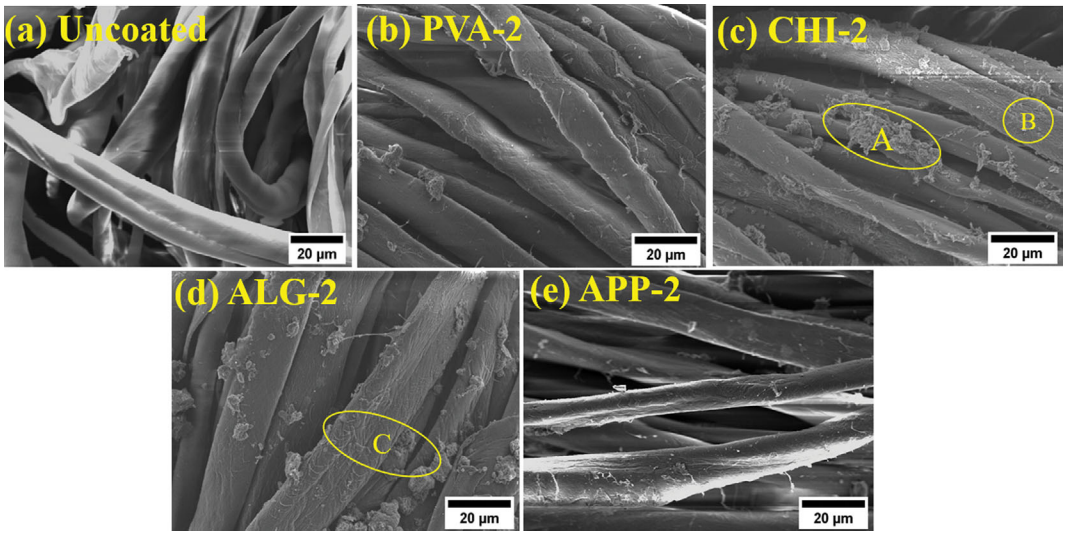

Fig. 2. (a)-(e) LV-SEM images of the uncoated and LBL-coated cotton samples.

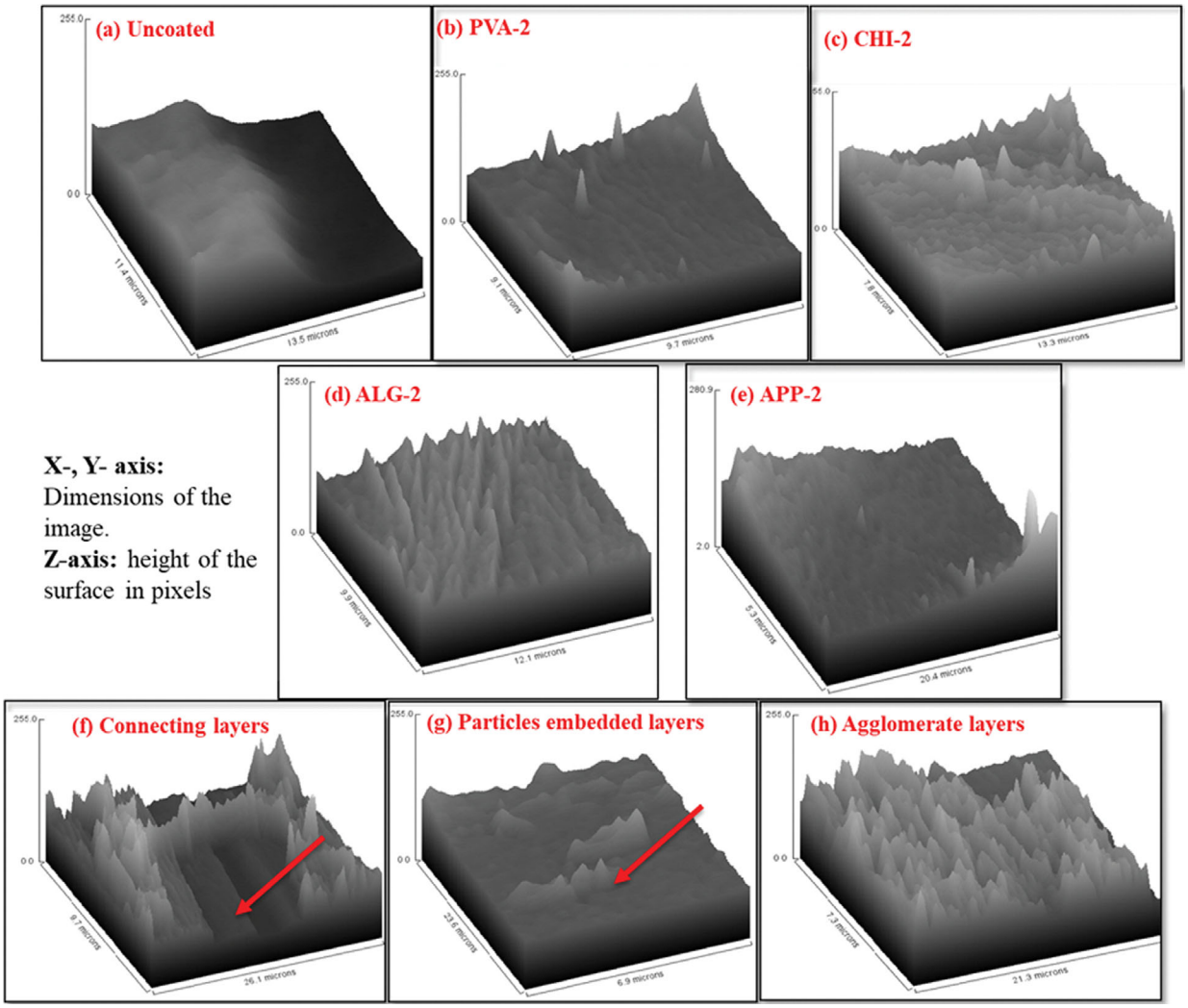

Fig. 3. 3D interactive plots of the uncoated and coated surfaces: (a) uncoated (b)-(e) coated samples (f) connecting layers (g) particle embedded layers (h) agglomerate layers.

material as encircled by the "C" and plotted in 3D as in Fig. 3(f). The fire resistant role of such phenomenon is still unknown; however, it could impart better mechanical connectivity to the char matrix in the aftermath of any burning event. Compared to other samples, the APP-2 surface is relatively uniform and free of agglomerated/precipitate components. Likewise, it can be further observed that compared to CHI-2 and ALG-2, the surface of the PVA-2 could be seen as having lesser extent of agglomeration and precipitation. The coated layers could also be seen to have engulfed the particles or the agglomerates as plotted in Fig. 3(g). Such embedded particles suggest that the agglomeration of the particles has occurred not only in the final stages, but also in the intermediate stages.

2. Elemental and Molecular Analysis

To know the elemental composition of the coating's layers, EDAX spectra of all the samples were obtained as shown in Fig. 4, and weight percentage of all the elements is listed in Table 1. The samples designated with a code ending in letter "B" are the after-burn samples. The coated samples, treated in various solutions, have different percentage of trace elements (Mg, Al, Si, Zr). All these trace

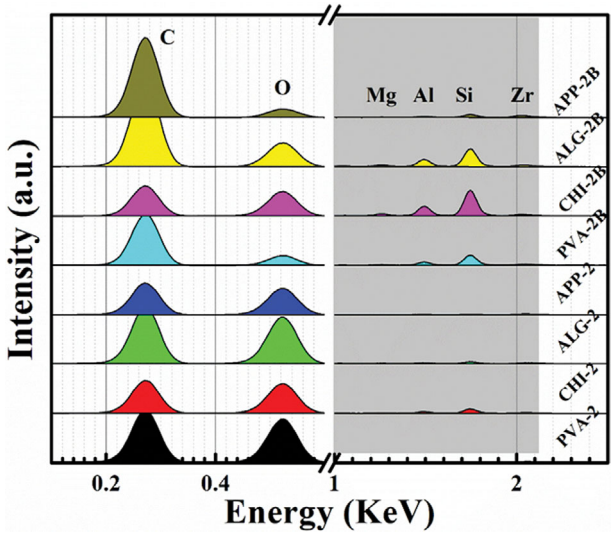

Fig. 4. EDAX analysis of the coated specimens: before burning and after burning.

Table 1. Elemental composition of the coated samples before and after burning process

#	PVA-2	PVA-2B	CHI-2	CHI-2B	ALG-2	ALG-2B	APP-2	APP-2B
C	49.58	70.49	48.80	47.72	50.20	66.18	58.55	79.27
O	49.58	15.57	42.97	25.84	47.44	19.92	40.47	13.21
Mg		0.40	4.27	3.02	3.42	2.55		
Al	0.19	2.26	1.32	5.42	1.39	2.84	0.14	0.62
Si	0.65	8.42	4.28	17.11	0.97	8.55	0.35	2.38
Zr		2.86	2.35	2.90			0.48	4.52

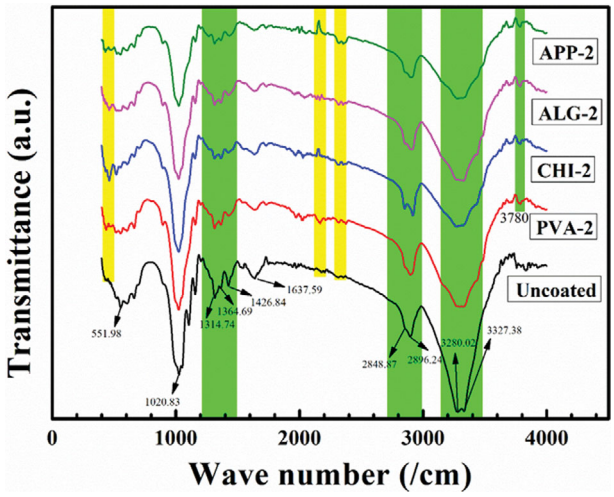

Fig. 5. AT-FTIR profile of the coated samples.

elements were absorbed onto the cotton fabric from the clay electrolytes solution. The concentrations of Mg, Al and Si are highest in CHI-2 followed by ALG-2, which suggests a higher uptake of clay components. However, for PVA-2 and APP-2, the content of clay materials could not reach maximal values. The presence of the clay component elements in the EDAX profile predicts enhanced fire-retardant performance of the cotton fibers, which is enhanced compared to the uncoated samples (control samples).

AT-FTIR spectra of the pre- and post-coated cotton fabric specimens were obtained to detect the deposited electrolytes entities (Fig. 5). Compared to the peaks profile of the uncoated cotton, additional peaks at 463.1 cm^{-1} and 3,785.6 cm^{-1} can be observed for the coated samples. Peaks obtained at 3,227 cm^{-1} correspond to the stretching vibration of the O-H, and can be seen as highly depressed and wider in the coated samples, suggesting the depiction of the O-H bonds due to the coated species occupancy. According to the Beer-Lambert law, the concentration of the specific components is linearly dependent on the absorption intensity of the specific wave numbers. Thus, a decrease in the peak intensity suggests decrease in the concentration of relevant component in the coating matrix. Likewise, the peaks correspond to the bending vibration of the -OH bend at 1,637.6 cm^{-1} are diminished [47]. The relatively inferior peak at 2,896.24 cm^{-1} was assigned to the C-H stretching vibration peak for the cotton fabric. Its intensity was increased for the CHI-2 due to the additional C-H bonds offered by chitosan, however sufficiently reduced in the case of APP-2. The additional peaks as indicated by the vertical yellow boxes such as at ~2,311.4 and 2,163.9 suggest the inflammable gases peaks (CO_2), which supports the fire resistive nature of coated substrate. The peaks corresponding to the flammable volatiles, such as carbonyl groups and ethers, were recorded at 1,637.6 (C=O), and 1,020.8 (C-O-C) were found with lower intensity than that of uncoated sample. The peak-lets obtained at 1,105.1 cm^{-1} and 1,427.3 cm^{-1} in the uncoated cotton were found missing and highly inhibited, respectively. Both of these peaks related to the C-O-C glycosidic band stretching vibrations, thus suggesting reduction in the flammability of the coatings.

3. Thermal Stability

Thermogravimetric analysis was carried out to analyze the degradation behavior of the uncoated and coated substrates as shown

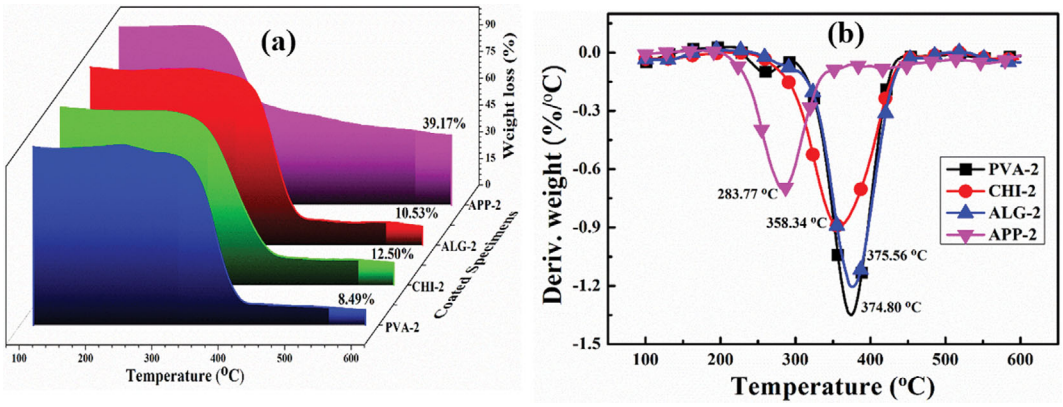

Fig. 6. Thermogravimetric analysis (a) Weight loss curves (b) and derivative curve of the samples.

Table 2. Thermogravimetric analysis parameters of then coated specimens

#	$T_{5\%}$	T_p, °C (DTG peak)	Residue at 600 °C (%)	Total decomposition (%)	Average decomposition rate (%/°C)
PVA-2	314.24	374.80	8.498	91.50	0.183
CHI-2	280.90	358.34	12.503	87.49	0.175
ALG-2	314.12	375.56	10.533	89.46	0.179
APP-2	255.28	283.77	39.17	60.83	0.122

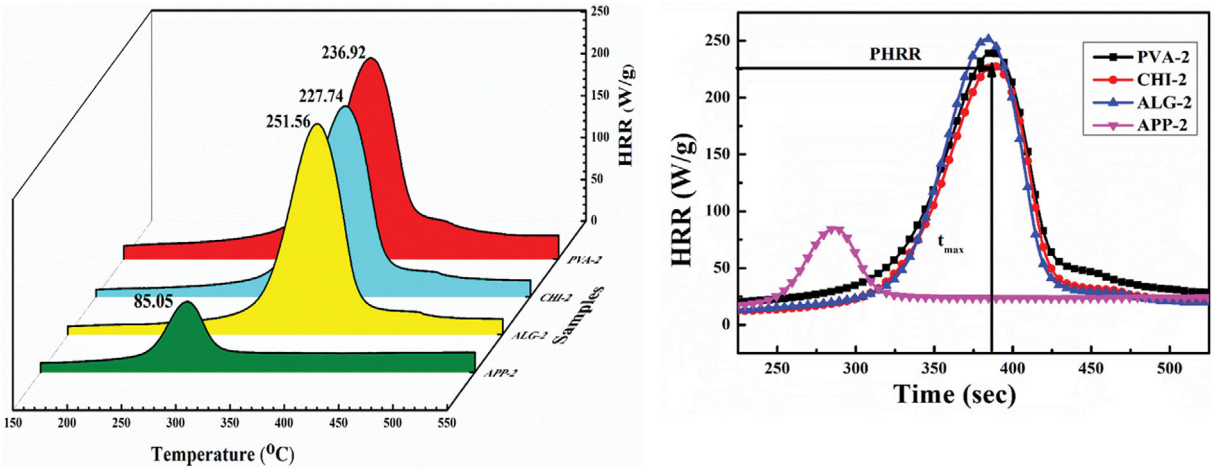

Fig. 7. Thermal parameters measured by micro-combustion calorimetry. (a) Heat Release Rate curves (HRR) and (b) Respective Total Heat Release (THR) values are those represented by the area under each curve.

in Fig. 6(a), (b). The maximum peak temperature at which degradation occurred was recorded as lowest for APP-2~ (283.8), followed by CHI-2~ (358) as can be seen in Fig. 6(b) and summarized in Table 2. This is rationalized due to the earlier degradation of the phosphorous content in APP-2 coating layers and nitrogen content CHI-2 layers. In the case of APP-2, the intermediate components such as phosphoric acid and polyphosphoric acid, formed due to thermal degradation of phosphorous constituents [48] could act as stimulus and promote the char layer formation thorough esterification and cross-linking reactions with cotton cellulose [11, 30]. Furthermore, the phosphoric acid component of the degraded APP could catalyze the carbonization of the cellulose fibers to form a stable carbon layer, which functioned as a physical barrier layer to protect underlying cotton fibers [49]. On the contrary, the nitrogen atom in the backbone of chitosan (CHI-2) can generate low-density incombustible gases, which could saturate the near-around zone of the combusting specimen, blocking oxygen from entering into active burning region and thus have a role as an oxygen blocker to inhibit the combustion process [50,51]. Thus, the degradation temperature recorded for ALG-2 and PVA-2 was higher compared to other samples. From the leftover mass residue as shown in Fig. 6(a), the average rate of decomposition was also decreased from 0.183%/°C to 0.122%/°C for APP-2, which suggests enhanced retardance by the APP-2. Generally, TGA curves can be divided into two regions; Region-1 (room temperature~ 350), Region-2 (350-600) as shown in Fig. 6(a). The behavior of thermal stability can be found different in these two regions; a gentle mass loss can be noticed in region-1, which is due to the breakdown of glycosidic bonds. While region-2 comprises the main combustion region, where a rapid loss of mass varied for each sample as PVA-2~ (91.5%), CHI-2~ (87.5%), ALG-2~ (89.5%), and APP-2~ (60.8%) was obtained. A two-step degradation can be observed for the samples, as indicated by the arrows in Fig. 6(a); however, small enough to be identified in the DTGA plot. The decompositions of the samples show the result of two competitive pathways: a) formation of the aliphatic char and b) volatile products. In region-2, it can be noticed that CHI-2 and ALG-2 have a greater resistance against decomposition, and by the increasing in temperature a smooth weight loss curve can be seen as in Fig. 6(a). The weight loss might have dependence on the remaining mass of the samples. This means that in region-2 the coated samples played a significant role through de-polymerizations, which caused the dehydration of glycosylic units to form thermally stable char.

4. Micro-combustion Calorimetry Analysis (MCC)

Using MCC, heat release rate (HRR) curves were obtained to analyze the thermal combustion behavior of the specimens on micro level as shown in Fig. 7(a). During the course of MCC, both the condense phase (pyrolysis) and gas phase (combustion) processes can be reproduced in a non-flaming manner. Though several properties, such as dripping, melting, swelling, charring, heat distortion, intumescence and incomplete combustion, cannot be fully scrutinized from the results obtained through milligram samples as in the MCC. However, the results can be compared with the macro thermal properties, such as flame test and cone calorimeter, and could provide significant thermal finger-prints of the samples. Results of the MCC are based on the loss of mass rate

and consumption of oxygen in the test. Considering the condensed phase model, the specific mass loss rate at temperature "T" for a constant heating rate β can be derived as [52].

$$\frac{-1}{m_0}\frac{dm}{dt} = \frac{\beta(1-\mu)}{eRT_{max}^2/E_a} = \frac{\beta(1-\mu)}{\Delta T_p} \quad (1)$$

In this equation "T_{max}" is the temperature at maximum mass loss/fuel generation rate, "e" is the natural number, and $\Delta T_p = eRT_{max}^2/E_a$ is the characteristic temperature interval over which pyrolysis occurs. Assuming the complete combustion of the volatiles produced during the pyrolysis in the MCC test, and invoking the oxygen consumption principle, the specific heat release rate (W/g-sample) can be obtained from oxygen consumption [52].

$$Q(t) = \frac{-h_{c,v}^0}{m_0}\frac{dm}{dt} = -\frac{C}{m_0}\frac{dr_0 m}{dt} = \frac{\rho CF}{m_0}\{\Delta O_2\}(t) \quad (2)$$

Thus, the specific heat release of a milligram sample can be obtained by the oxygen consumption analysis during the MCC test, through Eqs. (1)-(2). From the HRR profile, it can be seen that the peak value of the HRR was drastically shifted to a very lower value for APP-2. The coated cotton started to decompose earlier for APP-2 compared to other samples, which agrees with the TGA values. The major decomposition profile ranges from 240-390 for APP, while it shifts to a very higher values for all other samples as shown in Fig. 7(a), summarized in Table 3. The peak HRR value for APP-2 was recorded as ~85 W g^{-1}, which is 66% lower than the highest value (ALG-2). The PHRR value for all the samples can be ranked as APP-2(85.1)<CHI-2(227.7)<PVA-2(236.9)<ALG-2 (251.6). A small peak around 455 °C can also be seen in all the specimens, which is due to the oxidation of char. Total heat release was obtained from the time integration of the HRR curve as shown in Fig. 7(b). The lowest total heat release rate was found for APP-2 followed by CHI-2 together with enhanced charring capability as summarized in Table 3. Heat release capacity is a major parameter predicting both the thermal stability and combustion properties, on the basis of which flammability of the materials can be classified. Heat release capacity (HRC) is obtained as stated in Eq. (2), and directly from the average heating rate and combination of sample mass. Thus, it is more intrinsic in nature compared to other values, which are not totally independent. From Table 3 it can be seen that the values of HRC qualify with the TGA and HRR results. The lower the HRC values, implies the minimum content of heat by a sample and thus by burning, it will release the minimum amount of that heat content. The minimum values of HRC can be noticed for APP-2~294.1 J g^{-1} K^{-1}, followed by CHI-2~305.4 J g^{-1}·K^{-1}. However, there cannot be seen significant difference between the HRC values of both these samples, strongly suggesting the encouraging role of CHI-2 as a green material for fire protection.

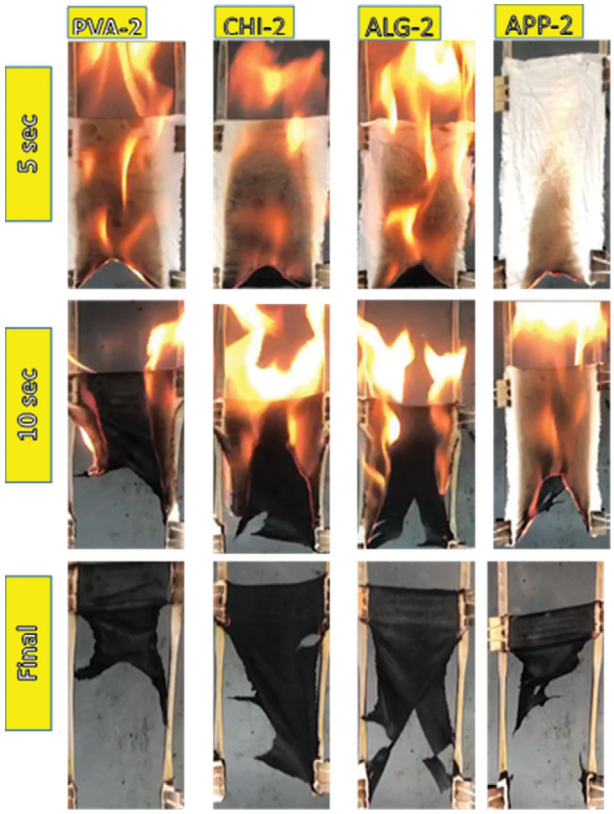

Fig. 8. Vertical flame (UL-94) test of the samples; images after 5 sec, 10 sec and final images of the char residue.

5. Flammability and After-burn Analysis

The flammability analysis was carried out using the UL-94 test, to correlate the macro-thermal properties with the micro-measurements as obtained using TGA and MCC. The vertical flame test was conducted on all the coated samples and optical images of the samples were taken after 5 sec and 10 sec of the flame burner removal as shown in Fig. 8. Final images were recorded after the complete burning of all the samples. It can be seen that though self-extinguishing did not occur; however, the flow of flame was effectively resisted by the coated samples. From the size, intensity and area covered by the flame at each specified time, it can be observed clearly that the APP-2 and CHI-2 resisted quite effectively at 5 sec, while the PVA-2 weakly resisted the flame followed by ALG-2. This can be further confirmed from the images at 10 sec, where the PVA-2 is totally burnt, while the CHI-2 and APP-2 are

Table 3. Resulting parameters of the samples after the micro-cone calorimetry test

#	PHRR (W/g)	T_{PHHR} (°C)	Range THR $_{max}$ (°C)	THR (KJ/g)	mo	mf	Char yield (%)	HRC (J/K·g)
PVA-2	236.92	378.11	300-450	19.73	12.7	0.9	7.08	406.15
CHI-2	227.74	379.54	300-450	17.17	16.8	1.5	8.92	305.42
ALG-2	251.56	379.63	300-450	17.36	17.3	1.2	7.05	318.51
APP-2	85.05	285.14	240-390	6.537	16.0	5.4	33.0	294.07

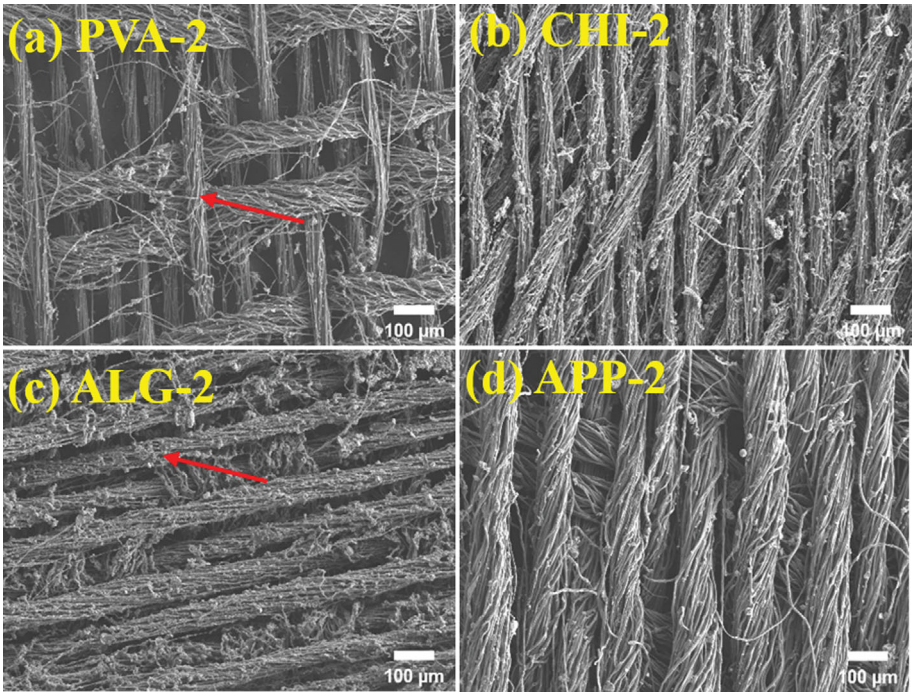

Fig. 9. (a)-(d) After-burn LV-SEM Surface morphologies of char residue.

still half way to burning completely. In addition, the burning time was recoded for each sample, which can be ranked as; PVA-2 (16 sec)<ALG-2 (18 sec)<CHI-2 (20 sec)<APP-2 (22 sec). Burning time is very important, which could be attributed to the escape time from the fire incident space, if there any incident happens. The longer burning time offers longer escape time, while the shorter burning time offers shorter escape time, which could be directly related to the damages caused by the fire.

The char obtained for CHI-2 is highest among all the samples, signifying its effectiveness against fire. Furthermore, there cannot be seen any significant damage to the char structure that remained intact. While all the other samples can be seen as broken, either partially or completely due to the strain caused by the burning reactions. Thus, the UL-94 test, which is more practical, acknowledges the effective role of green polymers coatings, i.e., CHI-2. Surface morphologies of the char samples obtained from the vertical flame test (UL-94 experiment) were analyzed using LV-SEM, as shown in Fig. 9. The leftover char residue and the debris amount can be observed through the images. The warp and weft morphology of the fabric can be evidently seen in the SEM images in the aftermath of burning. However, contraction, damages, broken portions and symmetrical disorder to some extent can also be observed on the surface of coated fabric. Further, it can be seen that the weave structure of the ALG-2 and PVA-2 was broken and disrupted more, as indicated by the arrows. The char debris can also be seen lying on the surface of the fabric fibers. Such debris acts as a stable char and can protect the fabric from further degradation. In comparison, the weave structure of the CHI-2 and APP-2 was not significantly damaged; however, the debris ratio in the CHI-2 can be seen as higher than the APP-2, signifying the effective role of the char against the flame. Peaks of the EDAX profile in the Fig. 4(e)-(h) suggest the inclusion of electrolyte particles in the debris to a sufficient extent.

6. Conclusion

Detailed micro and macro thermal investigation of the LBL-based bio (ca-alginate and chitosan) and synthetic-polymers (ammonium polyphosphate and polyvinyl alcohol) were carried out.

1. Microstructure of the bio-polymers based coatings was found to be comprised of (i) uniform layered structures, (ii) agglomerated/precipitated structures, (iii) particle embedded-structures and (iv) inter-fibers connecting layers structures, while only uniform layered structure was revealed for synthetic polymers coatings. The microstructural variations resulted due to the significant inter-electrolyte constituents interaction compared to the simple electrolyte-substrate interaction for the APP based system.
2. Despite thicker coatings obtained for the ALG-2, and CHI-2, the lowest decomposition rate was recorded for APP-2~60.83%, followed by CHI-2~87.49% at 600 °C obtained through TGA.
3. MCC result revealed lowest PHRR and THR values for APP~ (85.1 W g^{-1}, 6.53 KJ g^{-1}), and CHI-2~ (227.74 W g^{-1}, 17.17 KJ g^{-1}), respectively.
4. The VFT and after-burn SEM analysis was explored for CHI-2 and APP-2; high structural integrity, high char residue and better flame resistance were found for the CHI-2.
5. APP based coating appears to offer better intrinsic resistance to degradation and flame initiation, while the CHI-2 specimens could offer better extrinsic resistance against flame spread through strong mechanical integrity and greater char residue.

ACKNOWLEDGEMENTS

The Korea National Research Foundation grant funded by the Korean government endorsed this work (No. 2018R1A6A1A030

24509 and 2021R1I1A1A0105510212). D.G.C. acknowledges the KAIX program (KAIST), Professors Hee-Seung Lee and Young-Min Rhee (Dept. of Chem., KAIST) for financial assistance during the fiscal years of 2020 and 2021, and International Joint Usage Project with ICR, Kyoto University (2019-115 and 2020-124).

REFERENCES

1. W. D. Schindler and P. J. Hauser, *Chemical finishing of textiles*, Woodhead Publishing, United Kingdom (2004).
2. B. Nabil, C. Christine, V. Julien and A. Abdelkrim, *Chem. Eng. J.*, **351**, 328 (2018).
3. T. Chen, J. Hong, C. Peng, G. Chen, C. Yuan, Y. Xu, B. Zeng and L. Dai, *Carbohydr. Polym.*, **208**, 14 (2019).
4. W. Wang, J. Wang, X. Wang, S. Wang, X. Liu, P. Qi, H. Li, J. Sun, W. Tang and S. Zhang, *Prog. Org. Coat.*, **149**, 105930 (2020).
5. P. J. Wakelyn, N. R. Bertoniere, A. D. French, D. P. Thibodeaux, B. A. Triplett, M.-A. Rousselle, W. R. Goynes Jr., J. Vincent Edwards, L. Hunter, D. D. McAlister and G. R. Gamble, Cotton Fiber Chem. Technol., Taylor & Francis, United Kingdom (2007).
6. B. Hou, K. Song, Z. Ur Rehman, T. Song, T. Lin, W. Zhang, Y.-T. Pan and R. Yang, *ACS Appl. Mater. Interfaces*, **14**(12), 14805 (2022).
7. K. Song, B. Hou, Z. Ur Rehman, Y.-T. Pan, J. He, D.-Y. Wang and R. Yang, *Chem. Eng. J.*, **448**, 137666 (2022).
8. P. Reddy, G. Agathian and A. Kumar, *J. Radiat. Phys. Chem.*, **72**(4), 511 (2005).
9. H. Yuan, W. Xing, P. Zhang, L. Song and Y. Hu, *Ind. Eng. Chem. Res.*, **51**(15), 5394 (2012).
10. K. Xie, A. Gao and Y. Zhang, *Carbohydr. Polym.*, **98**(1), 706 (2013).
11. J. Alongi and G. Malucelli, *J. Mater. Chem.*, **22**(41), 21805 (2012).
12. J. Alongi, F. Carosio and G. Malucelli, *Polym. Degrad. Stabil.*, **106**, 138 (2014).
13. A.-L. Davesne, M. Jimenez, F. Samyn and S. Bourbigot, *Prog. Org. Coat.*, **154**, 106217 (2021).
14. K. M. Holder, R. J. Smith and J. C. Grunlan, *J. Mater. Sci.*, **52**(22), 12923 (2017).
15. O. Köklükaya, R.-M. P. Karlsson, F. Carosio and L. Wågberg, *J. Carbohydr. Polym.*, **255**, 117468 (2021).
16. C. K. Kundu, Z. Li, L. Song and Y. Hu, *Eur. Polym. J.*, **137**, 109911 (2020).
17. S. T. Lazar, T. J. Kolibaba and J. C. Grunlan, *Nat. Rev. Mater.*, **5**(4), 259 (2020).
18. P. Bertrand, A. Jonas, A. Laschewsky and R. Legras, *Macromol. Rapid Commun.*, **21**(7), 319 (2000).
19. G. Decher and J. B. Schlenoff, *Multilayer thin films: Sequential assembly of nanocomposite materials*, Wiley Online Library, Uniited States (2002).
20. F. Lv, Z. Peng, L. Zhang, L. Yao, Y. Liu and L. Xuan, *J. Liq. Cryst.*, **36**(1), 43 (2009).
21. Y. Shimazaki, R. Nakamura, S. Ito and M. Yamamoto, *Langmuir*, **17**(3), 953 (2001).
22. J. Sun, T. Wu, F. Liu, Z. Wang, X. Zhang and J. Shen, *Langmuir*, **16**(10), 4620 (2000).
23. G. Fleer, M. C. Stuart, J. M. Scheutjens, T. Cosgrove and B. Vincent, *Polymers at interfaces*, Springer Science & Business Media (1993).
24. M. Kweon, P. Bhirud and F. S. Saskatoon, *J. Starch-Stärke*, **48**(6), 214 (1996).
25. J. Addison, *Regul. Toxicol. Pharmacol.*, **21**(3), 397 (1995).
26. Y. C. Li, S. Mannen, A. B. Morgan, S. Chang, Y. H. Yang, B. Condon and J. C. Grunlan, *Adv. Mater.*, **23**(34), 3926 (2011).
27. J. Alongi, F. Carosio and G. Malucelli, *Polym. Degrad. Stabil.*, **97**(9), 1644 (2012).
28. F. Carosio, J. Alongi and G. Malucelli, *Carbohydr. Polym.*, **88**(4), 1460 (2012).
29. L.-l. Wang, T. Zhang, H.-q. Yan, M. Peng, Z.-p. Fang, Y. Li and W. Hao, *Chin. J. Polym. Sci.*, **32**(3), 305 (2014).
30. F. Carosio, C. Negrell-Guirao, A. Di Blasio, J. Alongi, G. David and G. Camino, *Carbohydr. Polym.*, **115**, 752 (2015).
31. K. Apaydin, A. Laachachi, V. Ball, M. Jimenez, S. Bourbigot and D. Ruch, *Colloids Surf. A: Physicochem. Eng. Asp.*, **469**, 1 (2015).
32. Z. Ur Rehman, S.-H. Huh, Z. Ullah, Y.-T. Pan, D. G. Churchill and B. H. Koo, *Carbohydr. Polym.*, **274**, 118626 (2021).
33. F. Carosio, J. Alongi, C. Paravidino and A. Frache, *Materials (Basel)*, **10**(7), 709 (2017).
34. T. Zhang, H. Yan, M. Peng, L. Wang, H. Ding and Z. Fang, *Nanoscale*, **5**(7), 3013 (2013).
35. Ş. S. Uğur, M. Sarıışık and A. H. Aktaş, *Mater. Res. Bull.*, **46**(8), 1202 (2011).
36. X. Wang, Y.-T. Pan, J.-T. Wan and D.-Y. Wang, *RSC Adv.*, **4**(86), 46164 (2014).
37. G. Laufer, C. Kirkland, A. B. Morgan and J. C. Grunlan, *Biomacromolecules*, **13**(9), 2843 (2012).
38. Y. Pan, J. Zhan, H. Pan, W. Wang, G. Tang, L. Song and Y. Hu, *ACS Sust. Chem. Eng.*, **4**(3), 1431 (2016).
39. T.-T. Yang, J.-P. Guan, R.-C. Tang and G. Chen, *Ind. Crops Prod.*, **115**, 16 (2018).
40. J. Alongi, R. A. Carletto, A. Di Blasio, F. Carosio, F. Bosco and G. Malucelli, *J. Mater. Chem. A*, **1**(15), 4779 (2013).
41. Z. U. Rehman, A. K. Niaz, J.-I. Song and B. H. Koo, *Polymers*, **13**(2), 303 (2021).
42. F. Carosio, G. Fontaine, J. Alongi and S. Bourbigot, *ACS Appl. Mater. Interfaces*, **7**(22), 12158 (2015).
43. Z. Ur Rehman, M. Kaseem, D. G. Churchill, Y.-T. Pan and B. H. Koo, *RSC Adv.*, **12**(5), 2888 (2022).
44. F. Bosco, R. A. Carletto, J. Alongi, L. Marmo, A. Di Blasio and G. Malucelli, *Carbohydr. Polym.*, **94**(1), 372 (2013).
45. J. Alongi, R. A. Carletto, F. Bosco, F. Carosio, A. Di Blasio, F. Cuttica, V. Antonucci, M. Giordano and G. Malucelli, *Polym. Degrad. Stabil.*, **99**, 111 (2014).
46. S. Basak, K. K. Samanta, S. Saxena, S. Chattopadhyay, R. Narkar, R. Mahangade and G. Hadge, *Polish J. Chem. Technol.*, **17**(1), 123 (2015).
47. Y. Luo, S. Wang, X. Du, Z. Du, X. Cheng and H. Wang, *Cellulose*, **28**(3), 1809 (2021).
48. I. van der Veen and J. de Boer, *Chemosphere*, **88**(10), 1119 (2012).
49. A. Abou-Okeil, S. M. El-Sawy and F. A. Abdel-Mohdy, *Carbohydr. Polym.*, **92**(2), 2293 (2013).
50. F. Fang, X. Chen, X. Zhang, C. Cheng, D. Xiao, Y. Meng, X. Ding, H. Zhang and X. Tian, *Prog. Org. Coat.*, **90**, 258-266 (2016).
51. S. Li, X. Lin, Z. Li and X. Ren, *Compos. Commun.*, **14**, 15 (2019).
52. R. Lyon, R. Walters, S. Stoliarov and N. Safronava, https://www.fire.tc.faa.gov/pdf/tc20-35.pdf (2013).